https://doi.org/10.5194/tc-2019-317
Preprint. Discussion started: 20 January 2020

The Cryosphere Discussions
Open Access
EGU

The Arctic Ocean Observation Operator for 6.9 GHz (ARC3O) - Part 1: How to obtain sea-ice brightness temperatures at 6.9 GHz from climate model output

Clara Burgard[1,2], Dirk Notz[1,3], Leif T. Pedersen[4], and Rasmus T. Tonboe[5]

[1]Max Planck Institute for Meteorology, Hamburg, Germany
[2]International Max Planck Research School for Earth System Modelling, Hamburg, Germany
[3]Institute of Oceanography, Center for Earth System Research and Sustainability, Universität Hamburg, Hamburg, Germany
[4]National Space Institute, Technical University of Denmark, Lyngby, Denmark
[5]Danish Meteorological Institute, Copenhagen, Denmark

Correspondence: Clara Burgard (clara.burgard@mpimet.mpg.de)

Abstract. We explore the feasibility of an observation operator producing passive microwave brightness temperatures for sea ice at a frequency of 6.9 GHz. We investigate the influence of simplifying assumptions for the representation of sea-ice vertical properties on the simulation of microwave brightness temperatures. We do so in a one-dimensional setup, using a complex 1D thermodynamic sea-ice model and a 1D microwave emission model. We find that realistic brightness temperatures can be simulated in winter from a simplified linear temperature profile and a self-similar salinity profile in the ice. These realistic brightness temperatures can be obtained based on profiles interpolated to as few as five layers. Most of the uncertainty resulting from the simplifications is introduced by the simplification of the salinity profiles. In summer, the simplified salinity profile leads to too high liquid water fractions at the surface. To overcome this limitation, we suggest using a constant brightness temperature for the ice during summer and to treat melt ponds as water surfaces. Finally, in our setup, we cannot assess the effect of snow properties during melting. As periods of melting snow with intermediate moisture content typically last for less than a month, our approach allows one to estimate reasonable brightness temperatures at 6.9 GHz from climate model output for about 11 months throughout the year.

1 Introduction

Sea-ice concentration products are retrieved from passive microwave brightness temperatures measured by satellites and come with a non-negligible uncertainty (Ivanova et al., 2015; Tonboe et al., 2016; Lavergne et al., 2019). This observational uncertainty hinders reliable climate model initialization (Bunzel et al., 2016) and model evaluation (Notz et al., 2013). Additionally, it hinders a robust extrapolation of the future sea-ice evolution based on current observations. For example, sea-ice area is strongly coupled to changes in the global-mean air temperature (Gregory et al., 2002; Winton, 2011; Mahlstein and Knutti, 2012; Ridley et al., 2012; Li et al., 2013) and thus to CO_2 emissions (Notz and Stroeve, 2016). The relationship between CO_2 emissions, global-mean air temperature and sea ice provides the possibility to project the future Arctic sea-ice evolution under different forcing scenarios. However, Niederdrenk and Notz (2018) showed that the observational uncertainty in sea-ice

https://doi.org/10.5194/tc-2019-317
Preprint. Discussion started: 20 January 2020

concentration translates into uncertainty in the sensitivity of sea ice to changes in global-mean air temperature and therefore leads to uncertainty in the temperature at which an ice-free Arctic in summer can be expected.

Observation operators are a current approach in climate science to circumvent observational uncertainty and the spread introduced by the use of retrieval algorithms on satellite measurements (Flato et al., 2013; Eyring et al., 2019). They simulate directly the observable quantity, in our case the brightness temperature, from the climate model output instead of retrieving the simulated quantity, in our case the sea-ice concentration, from the satellite observations. A sea-ice observation operator reduces the uncertainty introduced by assumptions used in retrieval algorithms about the state of other climatic variables besides the sea-ice concentration. It takes advantage of knowing the consistent climate state in time and space simulated by the climate model alongside the sea ice. This knowledge allows a more comprehensive approach to climate model evaluation, as we cannot only assess the simulated sea-ice concentration but also the simulated sea-ice temperature, snow cover, and sea-ice type. The feasibility and limitations of an observation operator applied to sea ice simulated by a climate model have not been investigated yet. This is the question we address here.

We investigate how important the complexity of the representation of sea-ice properties is for the simulation of sea-ice surface brightness temperatures emitted by different ice types. Experiments using a model accounting for part of the processes at work inside the sea ice combined with an emission model have shown that knowing the vertical sea-ice properties are sufficient to generate realistic microwave brightness temperatures (Tonboe, 2010; Tonboe et al., 2011). We mainly concentrate on the vertical representation of temperature and salinity inside the ice and snow, as they are the main drivers of the liquid brine fraction in the ice and liquid water fraction in the snow and thus of sea-ice brightness temperatures, especially at low microwave frequencies (Ulaby et al., 1986). As most general circulation models (GCMs) do not explicitly represent the time evolution of vertical profiles of temperature and salinity in the ice and snow, we investigate the effect of simplified temperature and salinity profiles on the simulation of brightness temperatures. We do so by comparing reference profiles, representing an estimate of reality, on the one hand and simplified profiles, representing GCM output, on the other hand in an idealized one-dimensional setup, using a complex thermodynamic sea-ice model and a microwave emission model.

We focus on the simulation of sea-ice brightness temperatures at 6.9 GHz at vertical polarization as a first step. At this frequency, the main driver of brightness temperatures are the sea-ice properties, while the contribution of the snow emission and scattering and of the atmospheric absorption and scattering due to water vapor, cloud liquid water and temperature are small compared to the surface contribution. The framework can, however, be extended to other frequencies and polarizations in the future, if the increasing importance of the snow and atmospheric contribution with increasing frequency is taken into account.

In Sec. 2, we provide the theoretical background about drivers of sea-ice brightness temperatures and in Sec. 3 we present our method and the sea-ice and emission models used. In Sec. 4, we explore the influence of simplifications in the temperature and salinity profiles on the simulation of sea-ice brightness temperatures to then explore the effect of a reduced number of layers in Sec. 5. To complete the study, we quantify the uncertainty introduced by a snow cover and the atmosphere in Sec. 6. Finally, we discuss our findings in Sec. 7 and conclude with suggestions for a functional observation operator for sea ice in Sec. 8. In our companion paper Burgard et al. (2019), we use these suggestions to construct the Arctic Ocean Observation

https://doi.org/10.5194/tc-2019-317
Preprint. Discussion started: 20 January 2020

Operator (ARC3O). We then evaluate the brightness temperatures simulated by ARC3O based on output of a coupled climate model against brightness temperatures measured by a satellite from space.

2 Theoretical background

The brightness temperature TB is a measure for the microwave radiation emitted by one medium or a combination of media and represents the temperature of a blackbody emitting the observed radiation. It is defined as:

$$\mathrm{TB} = \epsilon_{\mathrm{eff}} \cdot T_{\mathrm{eff}} \tag{1}$$

where ϵ_{eff} is the emissivity of the emitting part of the medium, i.e. the layers influencing the resulting radiation emitted at the surface and T_{eff} the integrated temperature over this same emitting part (Hallikainen and Winebrenner, 1992; Shokr and Sinha, 2015b; Tonboe, 2010). The thickness of the emitting part and its emissivity depend on the permittivity and scattering properties of the medium, which in turn depend on the medium and on the frequency and polarization of the radiation.

In the case of sea ice, the permittivity is mainly a function of the fraction and distribution of liquid water in the form of brine inside the ice as the permittivity of water is an order of magnitude higher than the permittivity of pure ice (Ulaby et al., 1986; Shokr and Sinha, 2015a). This means that water is a stronger absorber than pure ice in the microwave range. The liquid water fraction in the snow and brine volume fraction in the ice are a function of temperature and bulk salinity. Brine is present within the ice throughout the year. If the ice becomes multiyear ice, most of its brine will have drained and the brine volume fraction decreases substantially compared to first-year ice. In snow, liquid water is mainly present during melting periods. Also, the lowest layer of the snow can be saline, especially above first-year ice (Barber et al., 1998; Shokr and Sinha, 2015b), enabling the presence of liquid water at the base of the snow. However, the sea-ice model used in our setup (see Sec. 3.2) does not simulate salinities above zero for the snow layer. We therefore do not have a reference snow salinity and cannot consider saline snow in our study setup.

The scattering of the microwave radiation in sea ice is a function of the permittivity and the size of scatterers inside the ice, snow, and atmosphere. In first-year ice, the main scatterers are brine pockets, while in multiyear ice the main scatterers are air bubbles, as most of the brine will have drained out (Winebrenner et al., 1992; Tonboe et al., 2006; Shokr and Sinha, 2015a). While a dry atmosphere and dry snow cover have a low permittivity, they can still influence scattering for frequencies higher than 10 GHz (Mätzler, 1987; Barber et al., 1998). In ice, snow, and atmosphere, the scattering becomes increasingly important with increasing frequency (Tonboe et al., 2006) as the wavelength successively approaches the size of brine pockets, snow grains and atmospheric aerosols and droplets.

Sea-ice concentration retrievals are based on satellite measurements at frequencies ranging from 1.4 GHz to 91 GHz (Ivanova et al., 2014, 2015; Gabarro et al., 2017). In the following, we concentrate on radiation at 6.9 GHz and vertical polarization. This frequency is advantageous as, with a wavelength of approx. 4.3 cm, it is only slightly affected by scattering inside the ice, the snow, and the atmosphere. The brightness temperature at 6.9 GHz therefore mainly depends on the emission and absorption properties inside the ice rather than on the scattering properties. This is why our focus lies on the properties of the sea-ice

https://doi.org/10.5194/tc-2019-317
Preprint. Discussion started: 20 January 2020

column, rather than on the snow structure or the state of the atmosphere. The emitting part of the ice can be around 20 cm thick for first-year ice and around 50 cm thick for multiyear ice (Tonboe et al., 2006).

3 Method and Data

3.1 Method

Although a few GCMs use detailed sea-ice modules (Vancoppenolle et al., 2009; Bailey et al., 2018), most GCMs use very simple sea-ice models that do not resolve the properties driving absorption and scattering inside the ice and snow. The Max Planck Institute Earth System Model (MPI-ESM, Wetzel et al., 2012) is such a GCM. In MPI-ESM, sea ice is represented as flat sea ice, with very simple sea-ice properties: a sea-ice (bare ice) or snow (snow-covered ice) surface temperature, a constant sea-ice bottom temperature at -1.8 °C, and a constant salinity of 5 g/kg regardless of sea-ice type or age (Notz et al., 2013). It is not clear yet how these simplifications affect a brightness temperature simulated based on these properties.

To explore the importance of the vertical distribution of sea-ice properties on the simulation of brightness temperatures, we use an idealized one-dimensional setup. This one-dimensional setup works as follows. On the one hand, we use a one-dimensional thermodynamic sea-ice model to simulate our reference (see Sec. 3.2). It computes highly resolved vertical sea-ice profiles under a given atmospheric forcing. On the other hand, we simplify these reference profiles to emulate profiles that could be inferred from information given by MPI-ESM for the same conditions. These two sets of profiles can be used to simulate two sets of brightness temperatures with a microwave emission model (see Sec. 3.3). The two sets of resulting brightness temperatures can then be used to quantify the effect of the GCM simplification on the brightness temperature simulation, compared to our reference (Fig. 1).

In this setup, we can quantify the influence of each parameter separately on the simulated brightness temperature. We could have compared brightness temperatures simulated on the basis of MPI-ESM output directly to brightness temperatures measured by satellites. However, we would then have not been able to infer the contribution to the difference in brightness temperatures of fundamental differences between model and observations on the one hand, and the contribution of the differences in the resolution of the ice properties on the other hand.

3.2 SAMSIM

Our reference profiles are simulated by the 1D Semi-Adaptive Multi-phase Sea-Ice Model (SAMSIM, Griewank and Notz, 2013, 2015). This is a complex thermodynamical model simulating the evolution of a 1D sea-ice column under given surface forcing. It computes sea-ice temperature, salinity, and brine volume fraction profiles on a semi-adaptive grid, with a number of layers varying between 0 and 100. It includes most of the processes governing sea-ice growth and melt, and interactions between the ice and, if existent, its snow cover. It was developed to investigate the brine dynamics inside the ice. A detailed description of underlying equations and represented processes can be found in Griewank and Notz (2013) and Griewank and Notz (2015).

https://doi.org/10.5194/tc-2019-317
Preprint. Discussion started: 20 January 2020

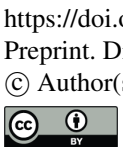

The Cryosphere Discussions
Open Access
EGU

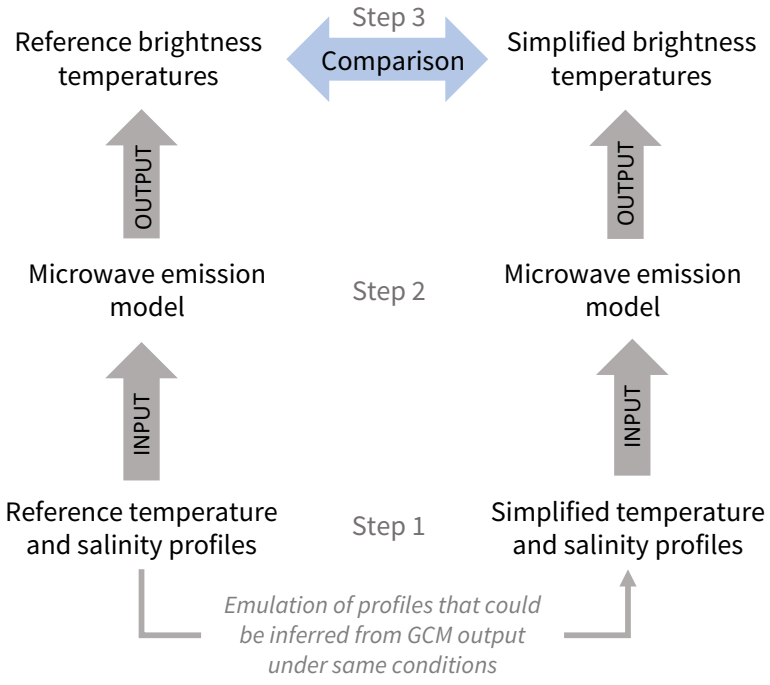

Figure 1. Schematic of the steps of our simulation and comparison method.

We force SAMSIM with 2 m air temperature, surface downward longwave radiation, surface downward shortwave radiation, and precipitation from the ERA-Interim reanalysis (Dee et al., 2011) in the time period from July 2005 to December 2009. This gives us insight into 4.5 annual cycles, so that we can assess the interannual variability of the growth and melt of sea ice and the evolution of its properties. The ocean salinity is kept at 34 g/kg and the oceanic heat flux at the bottom of the ice is derived from SHEBA measurements, varying between 0 W/m^2 in spring and 14 W/m^2 in autumn (Huwald et al., 2005; Griewank and Notz, 2015).

To gain insight into differences in microwave emission between first-year ice and multiyear ice, we focus on two points in the Arctic Ocean (Fig. 2). The first point represents first-year ice at 75°N00°W, where the ice always melts completely in summer in our SAMSIM simulations. The second point is at 90°N, where the ice survives the melt season and becomes multiyear ice from the second simulation year onwards. Note that in our setup the simulated sea-ice evolution is not necessarily representative for the real sea-ice evolution at that location. For example, sea ice seldom exists at 75°N00°W in reality. The presence of ice in this idealized simulation is likely linked to the oceanic heat flux used. This oceanic flux was measured in the SHEBA site north of Alaska and is very different than in the North Atlantic. However, this does not affect our study because we work in an idealized setup. Also, to ensure our results are robust, we have conducted the same analysis on five other points distributed in the Arctic Ocean (74°N170°E, 77°N39°E, 80°N160°W, 82°N120°W, 85°N50°W) and the results support our conclusions.

https://doi.org/10.5194/tc-2019-317
Preprint. Discussion started: 20 January 2020

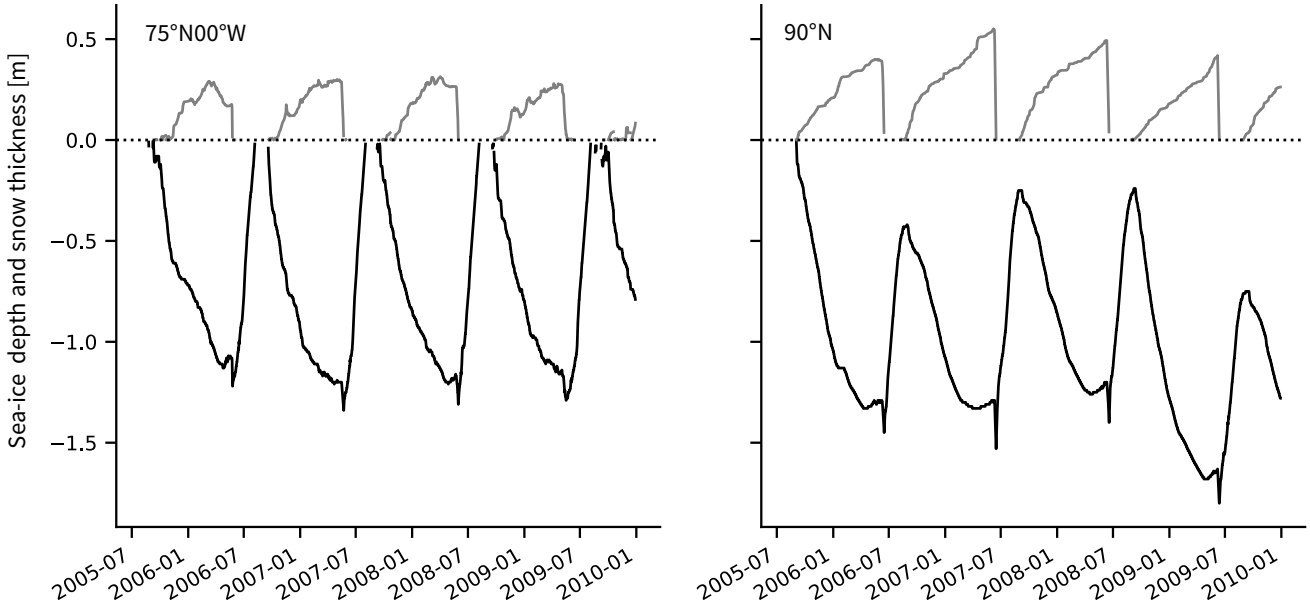

Figure 2. Evolution of sea-ice (black line) and snow (grey line) thickness as simulated by SAMSIM under ERA-Interim forcing between July 2005 and December 2009. The peaks in ice thickness during the snow melt period are a model artifact of SAMSIM, where snow melt occurs in the form of snow-to-slush conversion, briefly increasing the thickness of the top ice layer.

3.3 MEMLS

The simulation of sea-ice brightness temperatures is conducted with a slightly modified version of the Microwave Emission Model for Layered Snowpacks (MEMLS) extended to sea ice (Tonboe et al., 2006). MEMLS was first developed by Wiesmann and Mätzler (1999) to simulate brightness temperatures emitted by a snowpack composed of several layers and was later extended to sea ice (Tonboe et al., 2006). MEMLS uses the information of the properties of the ice and snow layers to simulate the path of microwave radiation from the bottom to the surface of the ice and, if present, snow. It uses the thickness, the temperature, the salinity, the density, the correlation length (measure for the scatterer size), the wetness, and information about the type of medium (snow, first-year/multiyear ice) of the different sea-ice and snow layers to compute absorption and scattering along the path. This then results in a brightness temperature emitted at the surface of the ice or snow.

Unless otherwise mentioned, we do not take into account the atmosphere in our analysis as its effect is relatively small at 6.9 GHz. The use of the term "brightness temperatures" in the following is therefore equivalent to the use of "brightness temperatures emitted at the surface of the ice and snow column".

https://doi.org/10.5194/tc-2019-317
Preprint. Discussion started: 20 January 2020

3.4 General simulation setup

The temperature and salinity profiles produced by SAMSIM are used as input for MEMLS for the simulation of brightness temperatures. Additionally, density profiles are derived from these properties using relationships given by Notz (2005) (see App. A). Next to the temperature, salinity and density profiles, other variables, which are not computed by SAMSIM, have to be provided to MEMLS. These are the correlation length, the incidence angle, the ocean temperature, the incoming microwave radiation from the atmosphere and the ice-ocean reflectivity for vertical polarization. They are set to constants, listed in Tab. 1.

Additionally, except for snow thickness and temperature, snow properties are neither resolved in SAMSIM nor in MPI-ESM. The main effect of snow on the radiation is its thermal insulation of the ice column and its refractive effect on the radiation induced by the difference in density between ice and snow and snow and atmosphere. The former is taken into account through the use of the SAMSIM snow thickness and snow temperature evolution, and the latter is taken into account through the snow thickness and by using a low density of snow compared to ice. We therefore set all snow properties, except the snow temperature and snow thickness, to constants, also listed in Tab. 1. In theory, the brightness temperature simulation is affected by the snow wetness if it is above zero. Neither SAMSIM or MPI-ESM resolve the liquid water fraction in the snow. In this study, we therefore set the snow wetness to zero. However, in a possible observation operator based on the results from this study, we strongly recommend to not consider periods of melting snow as we do not have the necessary information to simulate plausible brightness temperatures.

Table 1. MEMLS constant input details and properties of the snow layer.

Incidence angle	55°
Ocean temperature	-1.8 °C
Incoming microwave radiation from the atmosphere	0 K
Ice-ocean reflectivity for V-polarization	0.25
Correlation length first-year ice	0.35 mm for depth $<$ 20 cm,
	0.25 mm for depth $>$ 20 cm
Correlation length multiyear ice	1.5 mm
Snow thickness	as computed by SAMSIM
Snow density	300 kg/m^3
Snow correlation length	0.15 mm
Snow salinity	0 g/kg
Snow temperature	as computed by SAMSIM

Our input for the emission model, e.g. salinity, correlation length, brine pocket form, comes with uncertainties. These are mainly caused by a partial or complete lack of in-situ observations and the resulting low understanding of their evolution. We therefore recommend more observations of the ice properties combined with concurrent microwave radiation measurements.

https://doi.org/10.5194/tc-2019-317
Preprint. Discussion started: 20 January 2020

A few of such observations exist already, from both laboratory setting and in-situ, but they mainly focus on frequencies higher than 6.9 GHz (e.g. Grenfell et al., 1998; Jezek et al., 1998; Perovich et al., 1998; Hwang et al., 2007). With more combined observations at lower frequencies, we expect that the uncertainty in the brightness temperature simulation can be reduced in the future through further research and better understanding of the components introducing the uncertainty.

For example, a better understanding of the sea-ice salinity evolution would be of advantage. The salinity parametrization used in Sec. 4.3 is based on an "L-shape" of the salinity profile, while it is argued that the sea-ice salinity profile often resembles a "C-shape" or even a "Γ-shape" (Nakawo and Sinha, 1981; Shokr and Sinha, 2015a). Another parameter of uncertainty is the correlation length. Although it is a variable quite well understood and quantifiable for snow (Mätzler, 2002; Proksch et al., 2015; Lemmetyinen et al., 2018), its quantification in sea ice is not clear and its values not well known. On a similar note, MEMLS makes assumptions about the form of the brine pockets. In our study we assumed spherical brine pockets. However, it is known that the shape depends highly on the ice age and formation. An extensive summary of the brine pocket form can be found in Light et al. (2003).

Finally, the use of MEMLS as a sea-ice emission model is a source of uncertainty as well. Here again, the lack of measurements of the parameters needed for the brightness temperature simulation and of microwave radiation itself has inhibited a comprehensive evaluation of the sea-ice version of MEMLS simulations against reality. Still, it is accepted as one of the main tools for sea-ice brightness temperature simulations and has shown its strength in several previous studies (Tonboe, 2010; Tonboe et al., 2011; Willmes et al., 2014; Lee et al., 2017).

These uncertainties, however, only have a limited impact on the present study. We concentrate on a relative comparison, where we change temperature and salinity in the ice to understand their impact on the brightness temperature, but assumptions about correlation length and the form of brine pockets are the same in our reference and our simplified brightness temperature simulations. The uncertainties will therefore not impact the difference between the two sets of brightness temperatures. Additionally, in regard to the absolute values, Burgard et al. (2019) show that realistic brightness temperatures can be simulated by MEMLS using the above mentioned uncertain assumptions with slight tuning. The effect of the uncertainties therefore remains small when considering large scales.

4 The influence of vertical sea-ice properties

4.1 Brine volume fraction

Sea-ice brightness temperatures at 6.9 GHz are mainly driven by the distribution of liquid water in the form of brine inside the ice, as absorption plays a larger role than scattering at this frequency. We compute the ice surface brine volume fraction with Eq. A4 based on the ice surface temperature and salinity given by SAMSIM and find that this relationship is clearly visible in the brightness temperatures simulated based on the vertical profiles from SAMSIM output. The brightness temperatures show a strong dependence on the ice surface brine volume fraction, i.e. in the top ice layer of the profiles (Fig. 3a). If we concentrate the brightness temperature simulation on the ice layers, i.e. using only the ice layers of the snow and ice column as input to MEMLS, the relationship is even clearer (Fig. 3b).

https://doi.org/10.5194/tc-2019-317
Preprint. Discussion started: 20 January 2020

Especially above an ice surface brine volume fraction of 0.2, the brightness temperature at the ice surface is linearly related to the ice surface brine volume fraction (Fig. 3b). This means that no radiation signal from below the surface influences the brightness temperature but only the surface brine volume fraction matters. The brightness temperature transitions roughly linearly between brightness temperatures typical for ice (≈ 260 K) at an ice surface brine volume fraction of 0.2 and brightness temperatures typical for open water (≈160 K) at an ice surface brine volume fraction of 1. The properties inside the ice do therefore not influence the brightness temperature when the ice surface has a brine volume fraction higher than 0.2. In our SAMSIM profiles, these high surface brine volume fractions fractions occur predominantly in summer, i.e. from April to September. We therefore suggest that an ice surface brine volume fraction above 0.2 can be interpreted both as very wet ice or as a measure for the melt-pond fraction.

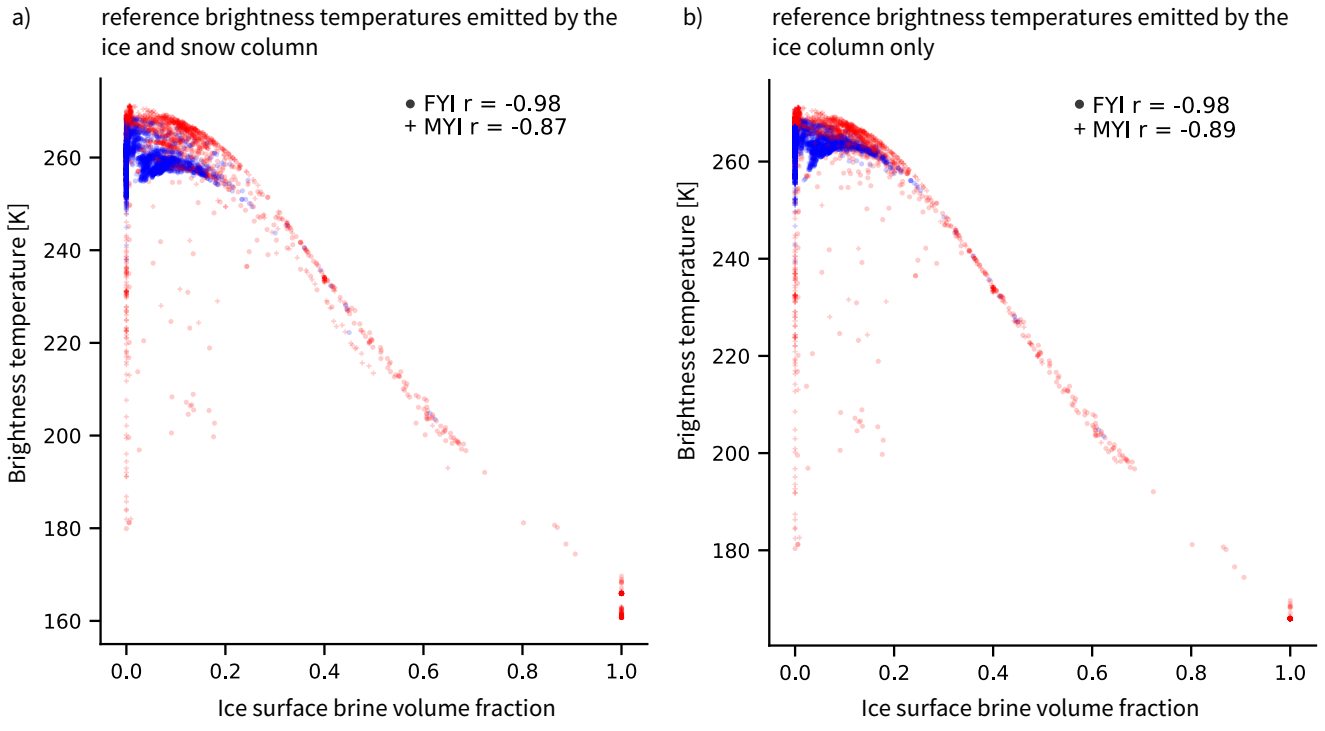

Figure 3. Reference brightness temperatures at 6.9 GHz, vertical polarization, simulated based on the (a) ice and snow column and on the (b) ice column only as a function of the reference ice surface brine volume fraction. Circles represent first-year ice (FYI), crosses represent multiyear ice (MYI). Blue is winter (October to March), red is summer (April to September). r is the correlation coefficient between the brightness temperature and the ice surface brine volume fraction for both ice types.

For surface liquid water fractions below 0.2, occurring in both winter and summer, the spread between brightness temperatures is 10 to 15 K for similar ice surface brine volume fractions. For these low ice surface brine volume fractions, the brightness temperatures are driven by the distribution of brine further inside the ice, which is a function of the temperature and

https://doi.org/10.5194/tc-2019-317
Preprint. Discussion started: 20 January 2020

salinity distribution. In some summer multiyear ice cases, the brightness temperature drops to ≈180 K. These low brightness temperatures occur in September when thin multiyear ice is entering the freezing period. Then, the simulated ice column has a brine volume fraction of zero except in the bottom layer. The radiation is therefore mainly influenced by the very saline bottom layer at the interface between ice and ocean, leading to low brightness temperatures. Unfortunately for the higher brightness temperatures around 260 K at low ice surface brine volume fractions, we could not infer a direct relationship between the brightness temperature and a given layer or a given brine volume fraction inside the ice from our data. We therefore proceed with sensitivity experiments to investigate the effect of simplifications in temperature and salinity profiles, and therefore in liquid water fraction profiles, on the simulated brightness temperature.

These sensitivity experiments demonstrate what happens when information about the vertical sea-ice profile lacks, as in the sea-ice representation by MPI-ESM. To this end, we compare brightness temperatures simulated based on SAMSIM profiles (in the following our reference) and brightness temperatures simulated based on simplified profiles (in the following our simplification). Our focus is on the influence of the ice properties on the brightness temperature. We therefore only use the ice layers of the ice and snow column as input for MEMLS. This way, the thermal insulation effect of the snow on the temperature profiles is conserved but the refraction at the ice-to-snow interface is neglected for the moment. This treatment corresponds to assuming that the snow is transparent to microwave radiation at this frequency. The refraction effect of the snow is discussed in Sec. 6.

The purpose of the sensitivity experiments is to identify the influence of the different profiles rather than the effect of differences in the vertical resolution, i.e. the number of ice layers. The simplified input profiles are therefore interpolated to the same number of layers as the reference profiles (ranging from 1 to 100 layers, depending on the ice thickness).

4.2 Linear Temperature and Constant Salinity

In a first experiment, we investigate the brightness temperature simulated based on information as would be given by MPI-ESM. For the simplified temperature profile, a two-step linear profile, we use the snow surface temperature as simulated by SAMSIM and infer the ice temperature at the interface between ice and snow from it, following Eq. A6. From this ice surface temperature, we interpolate linearly to the ice bottom layer, which has a temperature of -1.8 °C. For the salinity profile, MPI-ESM assumes a constant salinity of 5 g/kg. As this is clearly too high for multiyear ice (Ulaby et al., 1986), we assume a constant salinity of 5 g/kg for first-year ice and a constant salinity of 1 g/kg for multiyear ice in our simplified salinity profiles (see dashed lines in Fig. 4).

The influence of the simplifications is clearly different depending on the season. We therefore divide our results into winter (October to March, see Fig. 5) and summer (April to September, see Fig. 6). In winter, the simplified profiles produce brightness temperatures close to reference brightness temperatures for first-year ice, with a mean absolute difference of 3.2±7.6 K (Fig. 5, first row). For multiyear ice, the spread is higher and there is a tendency of simplified brightness temperatures to underestimate the reference brightness temperatures, with a mean absolute difference of 7.2±5.0 K.

In summer, the mean absolute differences are one order of magnitude higher, with 43.21±43.94 K for first-year ice and 43.02±45.73 K for multiyear ice (Fig. 6, first row). Simplified and reference brightness temperatures are clearly different most

https://doi.org/10.5194/tc-2019-317
Preprint. Discussion started: 20 January 2020

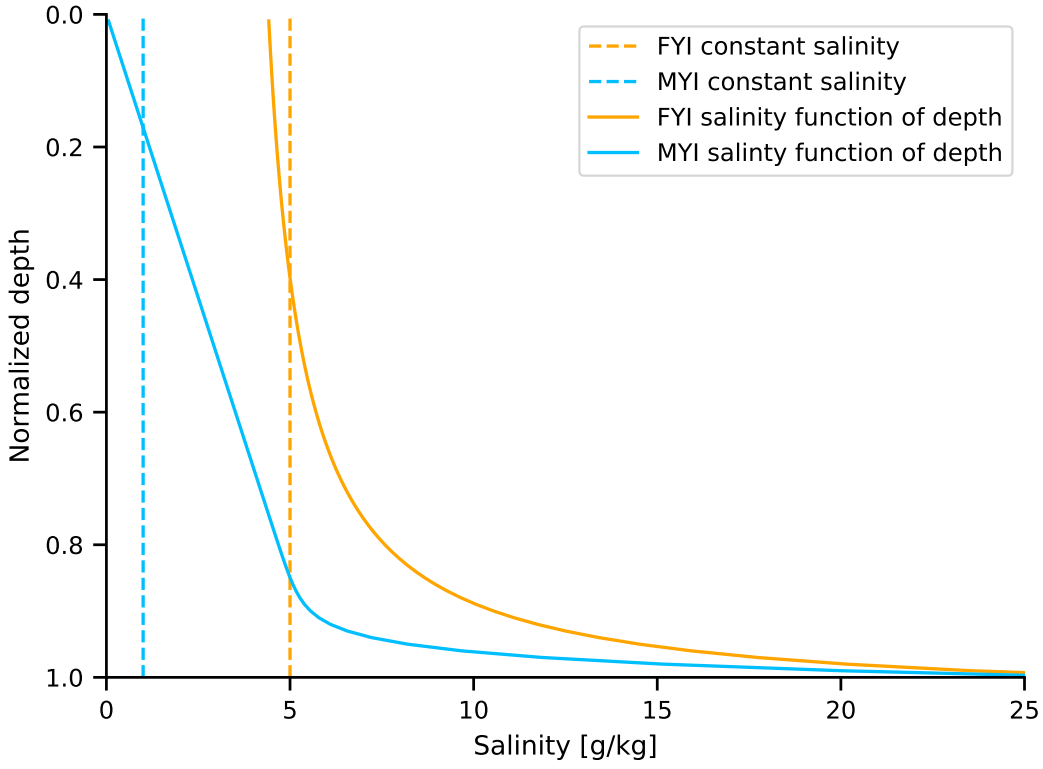

Figure 4. Salinity profiles used for the simplified profiles. FYI: First-year ice, MYI: Multiyear ice. The dashed lines represent the constant salinity profiles used in Sec. 4.2 and the full lines represent the salinity profiles as a function of depth used in Sec. 4.3

of the time. Especially, the simplified brightness temperature is close or equal to 160 K, i.e. open water brightness temperatures, at most of the time steps. This is because in summer, the physical temperature of the ice surface approaches 0 °C and, the closer it gets to 0 °C, the lower the salinity must be in order for dry ice to exist rather than slush. At high temperatures and salinities of 5 g/kg, the brine voume fraction therefore approaches 1 very fast, leading to low brightness temperatures. For multiyear ice, the effect of a salinity of 1 g/kg on the ice surface brine volume fraction is visible in a similar way.

To confirm our findings for summer and understand further our findings for winter, we conduct two additional sensitivity experiments. In the first experiment, the simplified brightness temperature is simulated based on the linear temperature profiles and the reference salinity profiles. In the second experiment, on the contrary, the simplified brightness temperature is simulated based on the reference temperature profiles and the constant salinity profiles. This enables us to separate the effect of the two simplifications. In both seasons, the effect of the constant salinity assumption is the main driver of the spread between the different brightness temperatures (Fig. 5 and Fig. 6, third row), while the linear temperature assumption has a small effect on the spread in winter and summer brightness temperatures (Fig. 5 and Fig. 6, second row).

https://doi.org/10.5194/tc-2019-317
Preprint. Discussion started: 20 January 2020

The Cryosphere
Discussions
Open Access
EGU

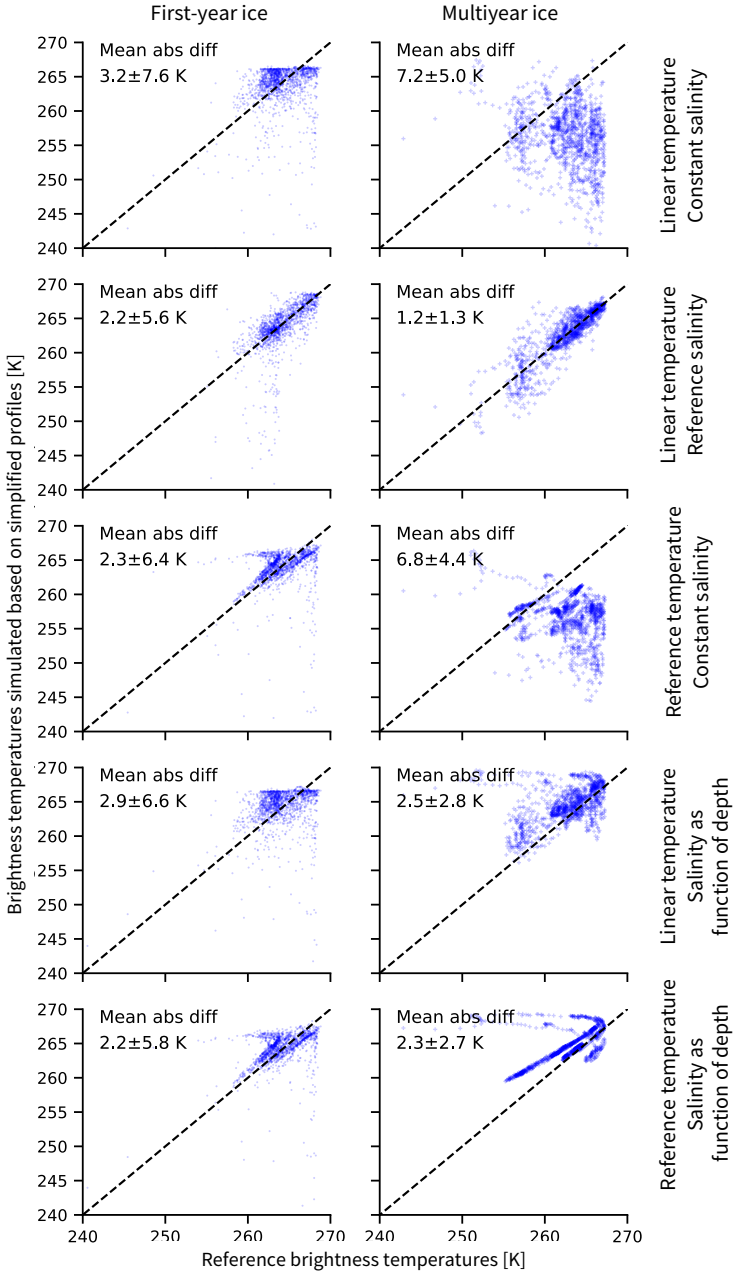

Figure 5. Brightness temperatures at 6.9 GHz, vertical polarization, simulated based on different simplified profiles as a function of reference brightness temperatures for winter. Left column: first-year ice, right column: multiyear ice. Note that the axes are limited to the range between 240 to 270 K for clarity. The remaining brightness temperatures are scattered between 165 and 240 K and represent around 2% of the simplified data and 0.4% of the reference data.

https://doi.org/10.5194/tc-2019-317
Preprint. Discussion started: 20 January 2020

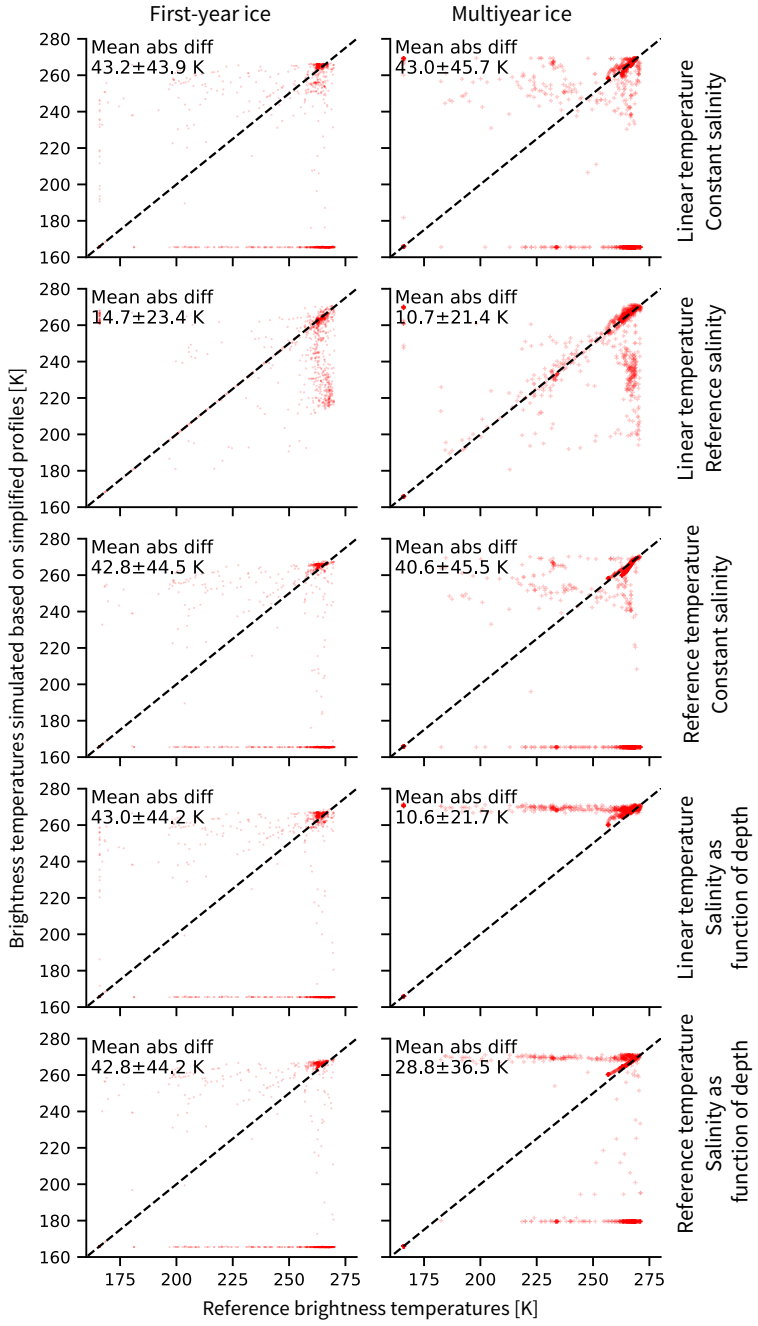

Figure 6. Brightness temperatures at 6.9 GHz, vertical polarization, simulated based on different simplified profiles as a function of reference brightness temperatures for summer. Left column: first-year ice, right column: multiyear ice.

https://doi.org/10.5194/tc-2019-317
Preprint. Discussion started: 20 January 2020

We therefore conclude that the assumption of a two-step linear temperature profile in the snow and ice does not introduce large uncertainties in the brightness temperature simulation. The assumption of constant salinity, however, introduces very large uncertainties in summer and smaller but still non-negligible uncertainties for multiyear ice in winter. We therefore explore another simplification approach for salinity profiles in a next step.

4.3 Linear Temperature and Salinity as a function of depth

An alternative approach to simplify salinity profiles is a parametrization representing salinity as a function of depth (Griewank and Notz, 2015). This parametrization assumes an L-shaped profile, with low salinity near the surface and a rapidly increasing salinity in the lower ice layers (see Fig. 4, full lines, and Tab. B1).

We now simulate the brightness temperature based on the linear temperature profiles and on the salinity profiles as a function of depth (Fig. 5 and Fig. 6, fourth row). With a mean absolute difference of 2.9±6.6 K in winter for first-year ice, the uncertainty is comparable to the constant salinity assumption. However, for multiyear ice, the uncertainty is reduced by around two thirds compared to the constant salinity, with a mean absolute difference of 2.5±2.8 K. In summer, the uncertainty is strongly reduced to 10.6±21.7 K for multiyear ice and stays comparable for first-year ice with 43.0±44.2 K. This represents a small improvement but the uncertainty remains too large in summer.

Again, if the brightness temperature is simulated based on reference temperature profiles and on the salinity profiles as a function of depth (Fig. 5 and Fig. 6, fifth row), it becomes clear that the assumption in the salinity profiles is the main driver for uncertainties in the brightness temperature simulations. However, using salinity profiles as a function of depth introduces less error than assuming the salinity to be constant throughout depth. We therefore recommend using a two-step linear temperature profile in snow and ice and an ice salinity as a function of depth when simulating brightness temperatures based on GCM output.

The effect of temperature and salinity distribution being clearer now, we turn to another characteristic of GCMs, the limited vertical resolution owing to computational efficiency. Indeed, computing vertical temperature and salinity profiles based on the surface temperature and sea-ice thickness given by a GCM adds a vertical dimension to a two-dimensional output. This means that the computation time and power needed by an operator applied to a GCM will be much higher than a one-dimensional setup. We therefore investigate the importance of the vertical resolution in a next step.

5 The influence of vertical spatial resolution

Applying an emission model to a GCM consumes high computation power, as the input profiles must be prepared and the emission model must be applied to many grid cells. In the case of the Arctic Ocean at the MPI-ESM low atmospheric resolution of 1.9°, this would mean for example ≈ 4000 data points per timestep. As ocean components in GCMs often have higher horizontal resolution than the atmosphere, this would mean even more computation power needed when using oceanic variables. Reducing the number of layers for the brightness temperature simulation is a possible aspect to reduce the computation time. This is the issue we explore in the following.

https://doi.org/10.5194/tc-2019-317
Preprint. Discussion started: 20 January 2020

The simplified profiles used for sensitivity experiments in Sec. 4 are interpolated to the same number of layers as the reference profiles, i.e. a variable number of layers depending on the ice thickness between one and 100 layers. We now run the brightness temperature simulation with the simplified profiles (linear temperature, salinity as a function of depth) interpolated on ten, seven, five, and three equidistant layers and compare the results to the reference brightness temperatures. We also include the experiment of Sec. 4 as an indicator for the minimal simplified uncertainty in the comparison. We concentrate on winter months, as we showed that the uncertainty in summer is already very large at high vertical resolution and mainly depends directly on the surface rather than on properties further inside the ice.

Table 2. Absolute mean difference and standard deviation [K] between simplified brightness temperatures simulated based on profiles interpolated on different number of layers and reference brightness temperatures simulated based on profiles covering 1 to 100 layers, depending on the thickness of the ice. These values only represent winter (October to March).

	3 layers	**5 layers**	**7 layers**	**10 layers**	**1 to 100 layers**
First-year ice	3.3±6.9	3.1±6.8	3.1±6.8	3.1±6.8	2.9±6.6
Multiyear ice	3.3±2.7	2.4±2.7	2.4±2.7	2.4±2.7	2.5±2.6

We find that the difference in uncertainty remains small between the reference simplification between 1 and 100 layers and the interpolation on ten, seven, or five layers, the mean uncertainty varying between 2.9 and 3.1 K for first-year ice and between 2.4 and 2.5 K for multiyear ice (see Tab. 2). Using three layers, the uncertainty increases slightly by 0.4 K for the former and by 0.8 K for the latter but still remains small. We therefore argue that using as few as five is as reasonable as 100 layers for the simulation of simplified brightness temperatures.

6 The influence of snow and atmosphere

Until now, we concentrated on the influence of sea-ice properties on the simulation of brightness temperatures emitted at the surface of the ice. These simulations included the thermal insulation effect of the snow but did not take into account the refraction effect of the snow cover on the radiation and the path of the radiation through the atmosphere. These are assumed to be small at 6.9 GHz. Nevertheless, it is of interest to quickly investigate the radiative effect of snow cover and atmosphere on the brightness temperature for uncertainty quantification and attribution.

We include the radiative effect of the snow cover in the brightness temperature simulation by using both snow and ice layers of the reference input profiles as input for MEMLS. Except thickness and temperature, which are computed by SAMSIM, all other variables are set to constants (Tab. 1), as neither SAMSIM nor MPI-ESM compute more details about the snow properties. Especially, we only consider dry snow in this study.

The main driver for the radiative effect of the dry snow cover is its density difference to the ice and atmosphere and its thickness. The density difference, and therefore the permittivity difference, between snow and ice on the one hand and between snow and atmosphere on the other hand leads to refraction of the radiation at its boundaries. The snow thickness also has an influence. A linear regression between snow thickness and differences between the simulated brightness temperatures with and

https://doi.org/10.5194/tc-2019-317
Preprint. Discussion started: 20 January 2020

without snow layer in winter gives a decrease by 0.13 K (0.13 K for first-year ice, 0.14 K for multiyear ice) for each cm of snow and an intercept of around -1.5 K (-1.7 K for first-year ice, -1.4 K for multiyear ice). This relationship only depends on the snow thickness and the density difference between snow and ice and between snow and atmosphere. It is independent of the snow temperature in our setup. In winter, using both ice and snow layers of the profile leads to a mean effect of -2.7±2.1 K for first-year ice and -3.8±2.4 K for multiyear ice on the brightness temperature compared to only using the ice layers of the profile. Although scattering is limited, the radiative effect of the snow cover hence remains important.

We consider only dry snow here as we do not know anything about the vertical profiles inside the snow from neither MPI-ESM nor SAMSIM. As liquid water and its distribution within the snow strongly affects the brightness temperature, we do not yet have a reliable solution to simulate the sea-ice brightness temperature when covered by wet snow.

We investigate the influence of the atmosphere with a similar approach as the influence of the snow cover. A simple atmospheric radiative transfer model developed by Wentz and Meissner (2000) is applied using the brightness temperatures simulated based on the reference ice and snow input profiles as the lower boundary conditions. The atmospheric effect mainly depends on the columnar liquid and water vapor content, which we again take from the ERA-Interim reanalysis, and on oxygen absorption, included in the radiative transfer model. Assuming a sea-ice concentration of 100%, the absolute mean impact of the atmosphere on the total brightness temperature is between 0.1 and 0.3 K between October and March, between 0.1 and 2 K between April and September.

7 Summary and Discussion

7.1 Winter brightness temperatures

We showed that in winter, sea-ice surface brightness temperatures simulated using a two-step linear temperature profile in ice and snow and an ice salinity as a function of depth as input for an emission model are comparable to sea-ice surface brightness temperatures simulated using complex temperature and salinity profiles. The remaining uncertainty is mainly driven by the simplification of the sea-ice salinity distribution. These realistic brightness temperatures can be reproduced with similar uncertainty using as few as five layers. A very high vertical resolution of the ice properties is therefore not needed. The refraction induced by the snow cover affects the brightness temperature, depending on its thickness, by 2.7 to 3.8 K. The atmosphere above the ice and snow column is negligible with an effect reaching at most 0.3 K at 100% sea-ice concentration.

This study was motivated by the fact that observational uncertainty could be reduced by the approach of an observational operator. It is however not trivial to evaluate this proposition based on our results. To compare the uncertainty [K] introduced by the brightness temperature simulation to uncertainties [%] introduced by a sea-ice concentration retrieval algorithm, we translate the uncertainty in brightness temperature into uncertainty in sea-ice concentration.

A simple retrieval algorithm to retrieve sea-ice concentration SIC is given by

$$\mathrm{SIC} = \frac{\mathrm{TB} - \mathrm{TB}_w}{\mathrm{TB}_i - \mathrm{TB}_w}, \tag{2}$$

https://doi.org/10.5194/tc-2019-317
Preprint. Discussion started: 20 January 2020

with TB the total brightness temperature (ice and open water combined), TB_w a typical open water brightness temperature, and TB_i a typical sea-ice brightness temperature. If we introduce uncertainties ΔSIC and ΔTB in the previous equation, this leads to

$$\mathrm{SIC} + \Delta\mathrm{SIC} = \frac{\mathrm{TB} + \Delta\mathrm{TB} - \mathrm{TB}_w}{\mathrm{TB}_i - \mathrm{TB}_w}, \tag{3}$$

resulting in

$$\Delta\mathrm{SIC} = \frac{\Delta\mathrm{TB}}{\mathrm{TB}_i - \mathrm{TB}_w}. \tag{4}$$

In our simulated reference brightness temperatures, TB_i, here the simulated brightness temperature for ice with low surface brine volume fraction, varies around 263 K (263.8±3.6 K for first-year ice and 263.7±4.3 K for multiyear ice) and TB_w, here the simulated brightness temperatures at very high surface brine volume fractions, varies around 166 K (166.1±0.7 K for first-year ice and 165.9±0.1 K for multiyear ice). Following Eq. 4, in this range spanning approximately 100 K, an uncertainty of 1 K in brightness temperature therefore approximately translates into 1% of absolute uncertainty in sea-ice concentration. The observational uncertainty of sea-ice concentration in winter is up to 2.5% in consolidated ice and up to 12% for marginal ice zones (Ivanova et al., 2015). The uncertainty of the simulated brightness temperatures translates to a similar range. This might, at first glance, not appear as a solution to drastically reduce the observational uncertainty. However, an observational operator is consistent in time and space and therefore allows a process-understanding of the uncertainties in brightness temperature simulations and, in a possible next step, in retrieval algorithms.

7.2 Spring and summer brightness temperatures

In summer, we cannot reproduce realistic sea-ice surface brightness temperatures due to the very high sensitivity of the liquid water fraction to small changes in salinity near 0 °C. We therefore recommend using another approach to simulate summer brightness temperatures. We suggest assuming that the brightness temperature of summer bare ice is similar all over the Arctic, as temperatures are near 0 °C. The surface brightness temperature is a linear combination of the bare ice brightness temperature and the brightness temperature of the melt ponds covering the ice. Therefore, this constant brightness temperature can be combined with open water brightness temperature, weighted by the fraction of melt ponds forming throughout the summer. This approach is simple. We have however not found any other approach that could come closer to reality as the sensitivities are very high near 0 °C.

Another problematic component when surface temperatures increase in spring and summer is the snow. While the detailed profile of dry snow is not needed as long as its presence is taken into account for the thermal insulation of the ice and for the refraction of the radiation, wet snow has a much higher influence on microwave emission. As in the case of melting snow, very precise information about the snow structure, e.g. wetness distribution, correlation length, and form of snow grains, are needed, we cannot come close to simulate realistic brightness temperatures from GCM output. In our experiments we have ignored this effect by setting the snow wetness to zero at all times. However, for an all-year-round realistic simulation of brightness temperatures, we suggest to exclude data containing melting snow from the brightness temperature simulation.

https://doi.org/10.5194/tc-2019-317
Preprint. Discussion started: 20 January 2020

7.3 Outlook

The evaluation framework in this study can be used to explore simulated brightness temperatures at higher frequencies, nearer to the most used operational frequencies. However, snow is a limiting factor in this case. While the radiative effect of the snow cover is small at 6.9 GHz, its impact increases with increasing frequency. It becomes therefore more important to know the snow structure, e.g. snow density, snow temperature, and snow scatterer structure. This information is lacking in GCMs. As the snow structure is more dynamic and changes faster than the ice structure, parametrization for the snow structure do not exist yet to our knowledge. It would be of high interest to explore the evolution of snow on sea ice in more details and perform sensitivity studies to identify possible simplifications. These could eventually lead to realistic brightness temperatures simulated based on GCM output at higher frequencies than 6.9 GHz.

Finally, our analysis focuses on the simulation of brightness temperatures based on output from a GCM which simulates sea ice with a very simple sea-ice model. The use of output from GCMs that simulate sea ice with more complex sea-ice models might yield lower uncertainty in the brightness temperature simulation. However, although these models compute many physical properties inside the ice, they do not necessarily store them for each time step. Using the more complex properties of these models would therefore require one to build the emission model into the model code, instead of applying an "external" operator to already produced model output.

8 Conclusions

With the help of a one-dimensional thermodynamic sea-ice model and a one-dimensional emission model, we investigated if realistic sea-ice brightness temperatures can be simulated based on GCM output at a frequency of 6.9 GHz with vertical polarization. We conclude that it is possible to simulate realistic sea-ice brightness temperatures depending on the time of year and on the boundary conditions.

We propose the following structure for an observational operator for sea ice at 6.9 GHz, vertical polarization:

- Periods of cold conditions: Use the temperature profile provided by the GCM if existing. Otherwise, use the simulated snow surface temperatur to infer the ice surface temperature and interpolate a linear temperature profile through the ice from there. Use the salinity profile provided by the GCM if existing. Otherwise, interpolate the salinity profile as a function of depth, following the functions given by Griewank and Notz (2015). Apply an emission model, e.g. MEMLS, to these profiles, combined with information about correlation length, sea-ice type, etc. Apply a simple ocean emission model and atmospheric radiative transfer model, e.g. Wentz and Meissner (2000), to account for the effect of open water when the sea-ice concentration is below 100% and for the effect of the atmosphere.

- Periods of bare ice near 0 °C: Use a constant brightness temperature for the ice surfaces. Burgard et al. (2019) derive a summer sea-ice surface brightness temperature of 266.78 from observational estimates. This represents a brightness temperature at the top of the atmosphere of 262.29 K corrected by the mean atmospheric effect of 4.49 K in their simulations. Weight this constant brightness temperature with the melt pond fraction. Apply a simple atmospheric radiative

https://doi.org/10.5194/tc-2019-317
Preprint. Discussion started: 20 January 2020

transfer model, e.g. Wentz and Meissner (2000), to account for the effect of open water when the sea-ice concentration is below 100% and for the effect of the atmosphere.

- Periods of melting snow: Ignore these points in the analysis. The GCM output does not provide enough information about the snow properties and wet snow strongly affects the brightness temperature.

The observational operator structure we present here allows us to simulate brightness temperatures from two-dimensional output by a GCM that can be compared with brightness temperatures measured by satellites. This opens new possibilities and perspectives for model-to-observation comparison in the Arctic Ocean.

Code and data availability. Primary data and scripts used in this study are archived by the Max Planck Institute for Meteorology and can be obtained by contacting publications@mpimet.mpg.de.

Appendix A: Retrieving sea-ice properties from temperature and salinity

The following formulas were used to compute the ice density ρ_i and brine volume fraction Φ_l profiles from the ice temperature T and salinity S profiles (Notz, 2005)

$$\rho_0 = 916.18 - 0.1403T \tag{A1}$$

where ρ_0 is the density of pure ice.

$$S_b = -17.6T - 0.389T^2 - 0.00362T^3 \tag{A2}$$

where S_b is the brine salinity.

$$\rho_w = 1000.3 + 0.78237S_b + 2.8008 \cdot 10^{-4} S_b^2 \tag{A3}$$

where ρ_w is the density of seawater.

$$\Phi_l = S/S_b \tag{A4}$$

$$\rho_i = \Phi_l \cdot \rho_w + (1 - \Phi_l) \cdot \rho_0 \tag{A5}$$

The following formula was used to infer the ice surface temperature $T_{\text{ice,surf}}$ from the snow surface temperature $T_{\text{snow,surf}}$:

$$T_{\text{ice,surf}} = \frac{T_{\text{snow,surf}} \cdot \frac{k_s}{h_s} + T_{\text{bottom}} \cdot \frac{k_i}{h_i}}{\frac{k_s}{h_s} + \frac{k_i}{h_i}} \tag{A6}$$

with k_s the thermal conductivity of snow (= 0.31 W/Km), k_i the thermal conductivity of ice (= 2.17 W/Km), h_s the snow thickness, h_i the ice thickness, T_{bottom} the temperature at the bottom of the ice, set to -1.8 °C.

https://doi.org/10.5194/tc-2019-317
Preprint. Discussion started: 20 January 2020

Appendix B: Salinity parametrization as a function of depth

Table B1. Formulas describing salinity as a function of depth as shown in the full lines in Fig. 4.

Ice type	**Salinity parametrization as a function of depth z**	**Constants needed**
First-year ice S_{fy}	$\frac{z}{a+bz} + c$	a = 1.0964, b = -1.0552, c = 4.41272
Multiyear ice S_{my}	$\frac{z}{a} + (\frac{z}{b})^{1/c}$	a = 0.17083, b = 0.92762, c = 0.024516
Transition first-year to multiyear ice	$(1-t) * S_{\text{my}}(z) + t * S_{\text{fy}}(z)$	t=0 at start of melt season and t=1 at start of freezing season

Author contributions. C.B. carried out all analyses and wrote the manuscript. D.N. and L.T.P. developed the original idea. All authors contributed to discussions.

Competing interests. No competing interests are present.

Acknowledgements. We thank Stefan Kern for constructive comments and discussions. This work was funded by the project "ESA CCI Sea Ice Phase 2".

https://doi.org/10.5194/tc-2019-317
Preprint. Discussion started: 20 January 2020

References

Bailey, D., DuVivier, A., Holland, M., Hunke, E., Lipscomb, B., Briegleb, B., Bitz, C., and Schramm, J.: CESM CICE5 Users Guide, Tech. rep., 2018.

Barber, D., Fung, A., Grenfell, T., Nghiem, S., Onstott, R., Lytle, V., Perovich, D., and Gow, A.: The role of snow on microwave emission and scattering over first-year sea ice, IEEE T. Geosci. Remote, 36, 1750–1763, https://doi.org/10.1109/36.718643, 1998.

Bunzel, F., Notz, D., Baehr, J., Müller, W., and Fröhlich, K.: Seasonal climate forecasts significantly affected by observational uncertainty of Arctic sea ice concentration, Geophys. Res. Lett., 43, 852–859, https://doi.org/10.1002/2015GL066928, 2016.

Burgard, C., Notz, D., Pedersen, L., and Tonboe, R.: The Arctic Ocean Observation Operator for 6.9 GHz (ARC3O) - Part 2: Development and evaluation, Submitted to The Cryosphere, 2019.

Dee, D., Uppala, S., Simmons, A., Berrisford, P., Poli, P., Kobayashi, S., Andrae, U., Balmaseda, M., Balsamo, G., Bauer, P., Bechtold, P., Beljaars, A., van de Berg, L., Bidlot, J., Bormann, N., Delsol, C., Dragani, R., Fuentes, M., Geer, A., Haimberger, L., Healy, S., Hersbach, H., Holm, E., Isaksen, L., Kållberg, P., Köhler, M., Matricardi, M., McNally, A., Monge-Sanz, B., Morcrette, J.-J., Park, B.-K., Peubey, C., de Rosnay, P., Tavolato, C., Thébaut, J.-N., and Vitart, F.: The ERA-Interim reanalysis: configuration and performance of the data assimilation system, Q. J. Roy. Meteor. Soc., 137, 553–597, https://doi.org/10.1002/qj.828, 2011.

Eyring, V., Cox, P., Flato, G., Gleckler, P., Abramowitz, G., Caldwell, P., Collins, W., Gier, B., Hall, A., Hoffman, F., Hurtt, G., Jahn, A., Jones, C., Klein, S., Krasting, J., Kwiatkowski, L., Lorenz, R., Maloney, E., Meehl, G., Pendergrass, A., Pincus, R., Ruane, A., Russell, J., Sanderson, B., Santer, B., Sherwood, S., Simpson, I., Stouffer, R., and Williamson, M.: Taking climate model evaluation to the next level, Nat. Clim. Change, https://doi.org/10.1038/s41558-018-0355-y, 2019.

Flato, G., Marotzke, J., Abiodun, B., Braconnot, P., Chou, S., Collins, W., Cox, P., Driouech, F., Emori, S., Eyring, V., Forest, C., Gleckler, P., Guilyardi, E., Jakob, C., Kattsov, V., Reason, C., and Rummukainen, M.: Evaluation of Climate Models, book section 9, pp. 741–866, Cambridge University Press, Cambridge, United Kingdom and New York, NY, USA, https://doi.org/10.1017/CBO9781107415324.020, 2013.

Gabarro, C., Turiel, A., Elosegui, P., Pla-Resina, J., and Portabella, M.: New methodology to estimate Arctic sea ice concentration from SMOS combining brightness temperature differences in a maximum-likelihood estimator, Cryosphere, 11, 1987–2002, https://doi.org/10.5194/tc-11-1987-2017, 2017.

Gregory, J., Stott, P., Cresswell, D., Rayner, N., Gordon, C., and Sexton, D.: Recent and future changes in Arctic sea ice simulated by the HadCM3 AOGCM, Geophys. Res. Lett., 29, 28–1–28–4, https://doi.org/10.1029/2001GL014575, 2002.

Grenfell, T., Barber, D., Fung, A., Gow, A., Jezek, K., Knapp, E., Nghiem, S., Onstott, R., Perovich, D., Roesler, C., Swift, C., and Tanis, F.: Evolution of electromagnetic signatures of sea ice from initial formation to the establishment of thick first-year ice, IEEE T. Geosci. Remote, 36, 1642–1654, https://doi.org/10.1109/36.718636, 1998.

Griewank, P. and Notz, D.: Insights into brine dynamics and sea ice desalination from a 1-D model study of gravity drainage, J. Geophys. Res-Oceans, 118, 3370–3386, https://doi.org/10.1002/jgrc.20247, 2013.

Griewank, P. and Notz, D.: A 1-D modelling study of Arctic sea-ice salinity, Cryosphere, 9, 305–329, https://doi.org/10.5194/tc-9-305-2015, 2015.

Hallikainen, M. and Winebrenner, D.: The Physical Basis for Sea Ice Remote Sensing, in: Microwave Remote Sensing of Sea Ice, edited by Carsey, F., chap. 4, pp. 29–46, American Geophysical Union, 1992.

Huwald, H., Tremblay, L.-B., and Blatter, H.: Reconciling different observational data sets from Surface Heat Budget of the Arctic Ocean (SHEBA) for model validation purposes, J. Geophys. Res. Oceans, 110, https://doi.org/10.1029/2003JC002221, c05009, 2005.

Hwang, B., Ehn, J., Barber, D., Galley, R., and Grenfell, T.: Investigations of newly formed sea ice in the Cape Bathurst polynya: 2. Microwave emission, J. Geophys. Res-Oceans, 112, C05 003, https://doi.org/10.1029/2006JC003703, 2007.

Ivanova, N., Johannessen, O. M., Pedersen, L. T., and Tonboe, R. T.: Retrieval of Arctic Sea Ice Parameters by Satellite Passive Microwave Sensors: A Comparison of Eleven Sea Ice Concentration Algorithms, IEEE T. Geosci. Remote, 52, 7233–7246, https://doi.org/10.1109/TGRS.2014.2310136, 2014.

Ivanova, N., Pedersen, L., Kern, S., Heygster, G., Lavergne, T., Sørensen, A., Saldo, R., Dybkjaer, G., Brucker, L., and Shokr, M.: Intercomparison and evaluation of sea ice algorithms: towards further identification of challenges and optimal approach using passive microwave observations, Cryosphere, 9, 1797–1817, https://doi.org/10.5194/tc-9-1797-2015, 2015.

Jezek, K., Perovich, D., Golden, K., Luther, C., Barber, D., Gogineni, P., Grenfell, T., Jordan, A., Mobley, C., Nghiem, S., and Onstott, R.: A broad spectral, interdisciplinary investigation of the electromagnetic properties of sea ice, IEEE T. Geosci. Remote, 36, 1633–1641, https://doi.org/10.1109/36.718635, 1998.

Lavergne, T., Macdonald Sørensen, A., Kern, S., Tonboe, R., Notz, D., Aaboe, S., Bell, L., Dybkjær, Eastwood, S., Gabarro, C., Heygster, G., Killie, M., Brandt Kreiner, M., Lavelle, J., Saldo, R., Sandven, S., and Pedersen, L.: Version 2 of the EUMETSAT OSI SAF and ESA CCI sea-ice concentration climate data records, Cryosphere, 13, 49–78, https://doi.org/10.5194/tc-13-49-2019, 2019.

Lee, S.-M., Sohn, B.-J., and Kim, S.-J.: Differentiating between first-year and multiyear sea ice in the Arctic using microwave-retrieved ice emissivities, J. Geophys. Res-Atm, 122, 5097–5112, https://doi.org/10.1002/2016JD026275, 2017.

Lemmetyinen, J., Derksen, C., Rott, H., Macelloni, G., King, J., Schneebeli, M., Wiesmann, A., Leppännen, L., Kontu, A., and Pulliainen, J.: Retrieval of Effective Correlation Length and Snow Water Equivalent from Radar and Passive Microwave Measurements, Remote Sensing, 10, 170, https://doi.org/10.3390/rs10020170, 2018.

Li, C., Notz, D., Tietsche, S., and Marotzke, J.: The Transient versus the Equilibrium Response of Sea Ice to Global Warming, J. Climate, 26, 5624–5636, https://doi.org/10.1175/JCLI-D-12-00492.1, 2013.

Light, B., Maykut, G., and Grenfell, T.: Applications of the interaction of microwaves with the natural snow cover, J. Geophys. Res.-Oceans, 108, https://doi.org/10.1080/02757258709532086, 2003.

Mahlstein, I. and Knutti, R.: September Arctic sea ice predicted to disappear near 2°C global warming above present, J. Geophys. Res-Atm, 117, https://doi.org/10.1029/2011JD016709, 2012.

Mätzler, C.: Applications of the interaction of microwaves with the natural snow cover, Remote Sensing Reviews, 2, 259–387, https://doi.org/10.1080/02757258709532086, 1987.

Mätzler, C.: Relation between grain size and correlation length of snow, J. Glaciol., 48, 461–466, https://doi.org/10.3189/172756502781831287, 2002.

Nakawo, M. and Sinha, N.: Growth Rate and Salinity Profile of First-Year Sea Ice in the High Arctic, J. Glaciol., 27, 315–330, https://doi.org/10.3189/S0022143000015409, 1981.

Niederdrenk, A. and Notz, D.: Arctic sea ice in a 1.5°C warmer world, Geophys. Res. Lett., 45, https://doi.org/10.1002/2017GL076159, 2018.

Notz, D.: Thermodynamic and Fluid-Dynamical Processes in Sea Ice, Ph.D. thesis, University of Cambridge, 2005.

Notz, D. and Stroeve, J.: Observed Arctic sea-ice loss directly follows anthropogenic CO_2 emission, Science, https://doi.org/10.1126/science.aag2345, 2016.

https://doi.org/10.5194/tc-2019-317
Preprint. Discussion started: 20 January 2020

Notz, D., Haumann, A., Haak, H., and Marotzke, J.: Arctic sea-ice evolution as modeled by Max Planck Institute for Meteorology's Earth system model, J. Adv. Model Earth Sy., 5, 173–194, https://doi.org/10.1002/jame.20016, 2013.

Perovich, D., Longacre, J., Barber, D., Maffione, R., Cota, G., Mobley, C., Gow, A., Onstott, R., Grenfell, T., Pegau, W., Landry, M., and Roesler, C.: Field observations of the electromagnetic properties of first-year sea ice, IEEE T. Geosci. Remote, 36, 1705–1715, https://doi.org/10.1109/36.718639, 1998.

Proksch, M., Löwe, H., and Schneebeli, M.: Density, specific surface area, and correlation length of snow measured by high-resolution penetrometry, J. Geophys. Res-Earth, 120, 346–362, https://doi.org/10.1002/2014JF003266, 2015.

Ridley, J., Lowe, J., and Hewitt, H.: How reversible is sea ice loss?, Cryosphere, 6, 193–198, https://doi.org/10.5194/tc-6-193-2012, 2012.

Shokr, M. and Sinha, N.: Sea ice Properties: Data and Derivations, in: Sea Ice: Physics and Remote Sensing, Geophysical Monograph 209, First Edition, edited by Union, A. G., chap. 3, pp. 99–137, John Wiley & Sons, Inc., 2015a.

Shokr, M. and Sinha, N.: Remote Sensing Principles Relevant to Sea Ice, in: Sea Ice: Physics and Remote Sensing, Geophysical Monograph 209, First Edition, edited by Union, A. G., chap. 7, pp. 271–335, John Wiley & Sons, Inc., 2015b.

Tonboe, R.: The simulated sea ice thermal microwave emission at window and sounding frequencies, Tellus, 62A, 333–344, https://doi.org/10.1111/j.1600-0870.2010.00434.x, 2010.

Tonboe, R., Andersen, S., Toudal, L., and Heygster, G.: Sea ice emission modelling, in: Thermal Microwave Radiation - Applications for Remote Sensing, edited by Mätzler, C., Rosenkranz, P., Battaglia, A., and Wigneron, J., pp. 382–400, IET Electromagnetic Waves Series 52, 2006.

Tonboe, R., Dybkjaer, G., and Højer, J.: Simulations of the snow covered sea ice surface temperature and microwave effective temperature, Tellus, 63A, 1028–1037, https://doi.org/10.1111/j.1600-0870.2011.00530.x, 2011.

Tonboe, R., Eastwood, S., Lavergne, T., Sørensen, A., Rathmann, N., Dybkjær, G., Pedersen, L., Høyer, J., and Kern, S.: The EUMETSAT sea ice concentration climate data record, Cryosphere, 10, 2275–2290, https://doi.org/10.5194/tc-10-2275-2016, 2016.

Ulaby, F., Moore, R., and Fung, A.: Passive microwave sensing of the ocean, in: Microwave Remote Sensing, Active and Passive Volume III, From Theory to Applications, chap. 18, pp. 1412–1521, Artech House, Inc., 1986.

Vancoppenolle, M., Fichefet, T., Goosse, H., Bouillon, S., Madec, G., and Morales Maqueda, M.: Simulating the mass balance and salinity of Arctic and Antarctic sea ice. 1. Model description and validation, Ocean Model., 27, 33–53, https://doi.org/10.1016/j.oceamod.2008.10.005, 2009.

Wentz, F. and Meissner, T.: Algorithm theoretical basis document (atbd), version 2, Tech. Rep. AMSR Ocean Algorithm, RSS Tech. Proposal 121599A-1, Remote Sensing Systems, Santa Rosa, CA, 2000.

Wetzel, P., Haak, H., Jungclaus, J., and Maier-Reimer, E.: The Max-Planck-Institute Global Ocean/Sea-Ice Model MPI-OM, Tech. rep., Max Planck Institute for Meteorology, 2012.

Wiesmann, A. and Mätzler, C.: Microwave emission model of layered snowpacks, Remote Sens. Environ., 70, 307–316, 1999.

Willmes, S., Nicolaus, M., and Haas, C.: The microwave emissivity variability of snow covered first-year sea ice from late winter to early summer: a model study, Cryosphere, 8, 891–904, https://doi.org/10.5194/tc-8-891-2014, 2014.

Winebrenner, D., Bredow, J., Fung, A., Drinkwater, M., Nghiem, S., Gow, A., Perovich, D., Grenfell, T., Han, H., Kong, J., Lee, J., Mudaliar, S., Onstott, R., Tsang, L., and West, R.: Microwave Sea Ice Signature Modeling, in: Microwave Remote Sensing of Sea Ice, edited by Carsey, F., chap. 8, pp. 137–175, American Geophysical Union, 1992.

Winton, M.: Do Climate Models Underestimate the Sensitivity of Northern Hemisphere Sea Ice Cover?, J. Climate, 24, 3924–3934, https://doi.org/10.1175/2011JCLI4146.1, 2011.